BNL-107324-2015-JA

AGU PUBLICATIONS

JGR

Journal of Geophysical Research: Atmospheres

RESEARCH ARTICLE
10.1002/2014JD022001

Special Section:
Fast Physics in Climate Models: Parameterization, Evaluation and Observation

This article is a companion to *Huang and Liu* [2014] doi:10.1002/2014JD022003.

Key Point:
- Statistical characteristics of observed cloud variability

Correspondence to:
D. Huang,
dhuang@bnl.gov

Citation:
Huang, D., E. Campos, and Y. Liu (2014), Statistical characteristics of cloud variability. Part 1: Retrieved cloud liquid water path at three ARM sites, *J. Geophys. Res. Atmos.*, *119*, 10,813–10,828, doi:10.1002/2014JD022001.

Received 7 MAY 2014
Accepted 18 AUG 2014
Accepted article online 20 AUG 2014
Published online 17 SEP 2014

Statistical characteristics of cloud variability. Part 1: Retrieved cloud liquid water path at three ARM sites

Dong Huang[1], Edwin Campos[2], and Yangang Liu[1]

[1]Brookhaven National Laboratory, Upton, New York, USA, [2]Argonne National Laboratory, Argonne, Illinois, USA

Abstract Statistical characteristics of cloud variability are examined for their dependence on averaging scales and best representation of probability density function with the decade-long retrieval products of cloud liquid water path (LWP) from the tropical western Pacific (TWP), Southern Great Plains (SGP), and North Slope of Alaska (NSA) sites of the Department of Energy's Atmospheric Radiation Measurement Program. The statistical moments of LWP show some seasonal variation at the SGP and NSA sites but not much at the TWP site. It is found that the standard deviation, relative dispersion (the ratio of the standard deviation to the mean), and skewness all quickly increase with the averaging window size when the window size is small and become more or less flat when the window size exceeds 12 h. On average, the cloud LWP at the TWP site has the largest values of standard deviation, relative dispersion, and skewness, whereas the NSA site exhibits the least. Correlation analysis shows that there is a positive correlation between the mean LWP and the standard deviation. The skewness is found to be closely related to the relative dispersion with a correlation coefficient of 0.6. The comparison further shows that the lognormal, Weibull, and gamma distributions reasonably explain the observed relationship between skewness and relative dispersion over a wide range of scales.

1. Introduction

Most of the physical processes related to clouds occur and interact with one another at scales smaller than the typical grid box of current climate models. The parameterizations used to represent these subgrid processes in climate models are generally formulated in terms of grid average (or in-cloud average) values of the relevant cloud properties. Because the processes in question are typically nonlinear functions of cloud properties, directly using grid average cloud properties to compute grid mean process rates without taking account for the corresponding subgrid-scale variation can lead to significantly biases in the calculated process rates [*Pincus and Klein*, 2000]. Probably, the most famous example is the systematic overestimation of cloud albedo by the plane-parallel homogeneous assumption [*Cahalan et al*., 1994]. The sign of the bias due to neglecting subgrid variability depends on whether the function representing the process is convex or concave [*Larson et al.*, 2001].

There is a wealth of literature examining the effects of subgrid cloud variability on microphysical processes and radiative transfer, using theoretical approaches, in situ aircraft observations, or satellite observations. *Barker et al.* [1996] and *Shonk et al.* [2010] evaluated the systematic biases in radiation calculations for various representations of cloud subgrid variability. *Pincus and Klein* [2000], *Larson et al.* [2001], and *Boutle et al.* [2013] attempted to demonstrate the importance of inclusion of subgrid cloud variability for accurate calculations of microphysical rates. *Griffin and Larson* [2013] derived analytical schemes for upscaling local microphysical processes; *Griffin and Larson* [2013] further demonstrated using large eddy simulations that the new analytical schemes increase autoconversion of cloud droplets to raindrops and accretion of cloud droplets onto raindrops. As a result, modern global climate models (GCMs) start to include the correction of the subgrid variability biases of microphysical process rates [*Morrison and Gettelman*, 2008] and radiative transfer, either via scaling of the cloud water content [e.g., *Cahalan et al.*, 1994] or Monte Carlo methods [e.g., *Pincus et al.*, 2003].

Although it is now widely recognized that the representation of cloud subgrid variability has significant effects on GCM radiation and microphysical calculations, studies on how to represent the cloud subgrid variability to minimize the radiative and microphysical biases [*Kim et al.*, 2005; *Wood and Hartmann*, 2006] are limited. As summarized by *Tompkins* [2002], various probability density functions (PDFs) have been used in GCMs to represent cloud variability. Univariate Gaussian and gamma distribution functions were proposed,

Figure 1. Locations of the DOE Atmospheric Radiation Measurement Program's three permanent sites: Southern Great Plains (SGP), tropical western Pacific (TWP), and North Slope of Alaska (NSA).

respectively, by *Zhang et al.* [2002] and *Morrison and Gettelman* [2008] to improve the consistency between cloud microphysical parameterizations. *Larson and Griffin* [2012] proposed to use a multivariate lognormal distribution to describe spatial subgrid variation of clouds. *Hill et al.* [2012] provided a global estimate of this subgrid variability for ice clouds, parameterizing it in terms of grid box size and cloud fraction using CloudSat products. The exact distribution of cloud condensate within GCM gridbox is almost certainly dependent on many aspects of the atmospheric state. While it is infeasible to fully resolve subgrid cloud PDF, it is possible to estimate the first few statistical moments of the PDF based on high-order turbulence closure [*Golaz et al.*, 2002; *Tompkins*, 2002]. If a functional form (e.g., the Gaussian distribution or the gamma distribution) of the PDF is assumed, the subgrid cloud PDF can then be readily derived using the estimated statistical moments. However, there is no general agreement as to which distribution function should be used to describe the PDF.

Furthermore, studies have revealed that many parameterizations have strong scale dependence, and because of the way cloud parameterizations are formulated, they are likely to be the most sensitive to scale dependence issues. For instance, the strong scale dependence of many cumulus schemes arises from the use of parcel models that are a strong function of vertical velocity, e.g., the Kain–Fritch scheme [*Kain and Fritsch*, 1990; *Kain*, 2004]. However, studies on scale dependence are rare, perhaps because long-term global cloud observations required for examining cloud subgrid variability and its scale dependence to guide parameterization development are very limited. The Atmospheric Radiation Measurement Program (ARM) of the Department of Energy (DOE) provides decade-long observations of cloud liquid water path (LWP) at its three permanent sites, each representing a different climate [*Stokes and Schwartz*, 1994]. Cloud LWP is a key parameter determining cloud radiative effects in GCMs and is one of the most extensively validated retrievals among the ARM Program. This study focuses on the characterization of the statistical properties of cloud LWP spatial variability as a function of scale and attempts to answer the question as to what is the best PDF for describing the subgrid variability by the use of the long-term observations collected by the DOE ARM Program at different sites.

The remainder of this paper is organized as follows. Section 2 provides a general description of the data used in this study. Section 3 explores the dependence of the first three statistical moments of observed cloud LWP on scale (or averaging window size). Section 4 examines the probability distribution of the observed statistical moments of cloud LWP at the scale of current GCM grid sizes. The relationship between these moments is explored in section 5. Section 6 evaluates if commonly used distribution functions can reproduce the observed relationship between the statistical moments. Section 7 summarizes the findings of this study.

2. Data and Methods

The data used in this study are based on the measurements of vertically pointing microwave radiometers operated by the U.S. DOE ARM program. For almost 2 decades, the ARM Program has operated two-channel microwave radiometers at its Southern Great Plains (SGP), tropical western Pacific (TWP), and North Slope of Alaska (NSA) sites. The TWP, SGP, and NSA sites are, respectively, located in tropical, midlatitude, and arctic regions to collect cloud, aerosol, and radiation data in diverse climate regimes (Figure 1). Satellite-based cloud retrievals provide better spatial coverage, but they rely on various assumptions about cloud droplet size distribution or surface emissivity variability [*Minnis et al.*, 2011]. Ground-based retrievals are widely used to validate satellite cloud retrievals [*Dong et al.*, 2008]. Ground and satellite retrievals are complimentary to each other in terms of spatial/temporal coverage and resolution.

The DOE ARM microwave radiometers measure downwelling radiance at frequencies of 23.8 and 31.4 GHz, and the measurements are used to retrieve column water vapor amount and liquid water path (LWP). The datastream used in this study is the 20 s Microwave Water Radiometer: Water Liquid And Vapor Along Line of Sight Path ("MWRLOS") retrieval product during 1999 to 2012. The MWRLOS retrieval is based on a statistical algorithm [*Liljegren et al.*, 2001] that uses a radiative transfer model to derive a set of retrieval coefficients, typically from a climatological data set of thermodynamic profiles from the nearby deployment site [*Cadeddu et al.*, 2013]. The accuracy of the LWP retrieval is within 0.03 mm according to the product document, and values below 0.03 mm could be considered as clear-sky conditions (ARM microwave radiometer handbook [*Morris*, 2006]). For clouds containing supercooled liquid, the retrieval uncertainty can be much higher due to poor knowledge about the microwave absorption coefficient of supercooled liquid water droplets [*Kneifel et al.*, 2014]. Supercooled liquid cloud layers are widely found at the NSA site [*Shupe et al.*, 2008]. The data corresponding to clear sky are excluded from the analysis of this study. To detect clear-sky period, we mainly use the Active Remote Sensing of Clouds (ARSCL) products that are based on cloud radar and lidar observations [*Clothiaux et al.*, 2000]. When the ARSCL data are not available, the MWRLOS product is used, and data points with LWP < 0.03 mm are labeled as clear. We performed some sensitivity tests to examine the effects of using different threshold values for clear-sky definition. Our results show that the choices of this threshold value are not sensitive since the ARSCL products are available at more than 70% of the times. It is well known that the measurements become unreliable when the dome of the radiometer gets wet (e.g., rain, melting snow, or dew). We therefore use the precipitation flag in the MWRLOS product to screen out the data contaminated by a wet dome. The values higher than 3.0 mm are also excluded from this study, since they are likely to have large uncertainties caused by precipitation contamination [*Liljegren et al.*, 2001]. It should be noted that the exclusion of very high LWP values could potentially result in an underestimation of the tail of the LWP distribution.

Strictly speaking, the LWP time series is a convolution of both spatial and temporal variation of clouds. A common approach to infer cloud spatial variability from vertically pointing observations is to invoke the Taylor's hypothesis [*Sun and Thorne*, 1995; *Powell and Elderkin*, 1974]. Taylor's hypothesis states that when the local turbulence is small compared with the mean advective flow (i.e., the mean wind), the covariance in time is related to the covariance in space by the speed of the mean wind [*Taylor*, 1938; *Burghelea et al.*, 2005]. For cloud fields, Taylor's hypothesis seems to apply in most cases [*Sun and Thorne*, 1995]. Recent advances in scanning sensors, e.g., scanning radiometers, and volume scanning radars enable direct evaluation of the Taylor's hypothesis [*Huang et al.*, 2008; *Kneifel et al.*, 2009; *Battaglia et al.*, 2010; *Schween et al.*, 2011], and this is out of scope of this study. We assume the validity of Taylor's hypothesis and interpret the observed temporal cloud variability as cloud spatial variability accordingly. Assuming the validity of the Taylor's hypothesis, the terms grid, gridbox, or averaging window are interchangeably used throughout this paper for convenience of presentation.

3. Scale Dependence of the Statistical Moments

Cloud variability at different spatial scales is a result of various physical processes. It is almost safe to assume that in the near future, most climate models will be able to have access to only several low-order statistical moments of subgrid cloud properties based on prognostic or diagnostic equations. Therefore, to a large extent, cloud subgrid variability has been, and will likely continue to be, parameterized in terms of several low-order statistical moments in GCMs. Furthermore, GCM grid sizes have evolved from several hundred kilometers to subhundred kilometers in the past few decades, and this trend shows no sign of stopping. Even high-resolution models, such as cloud-resolving and large-eddy simulation models, require parameterization of processes that occur over the scales smaller than their grid spacings. Thus, this section examines the variation of the first three statistical moments of cloud LWP, i.e., mean, standard deviation, and skewness, as a function of gridbox size as measured by the averaging window size.

Figure 2 shows the mean statistical moments of cloud LWP as a function of averaging window size for the TWP, SGP, and NSA sites. The statistical moments are first calculated in each averaging window, and the mean moments are then computed for all-cloudy windows. The mean time-average LWP is almost constant at each site and fluctuates, respectively, around 0.20, 0.18, and 0.13 mm across a large range of window size from a few minutes to 2 days for TWP, SGP, and NSA, respectively. This is an expected result since the mean time-average LWP only depends on the total liquid water amount in the entire period. The NSA site has

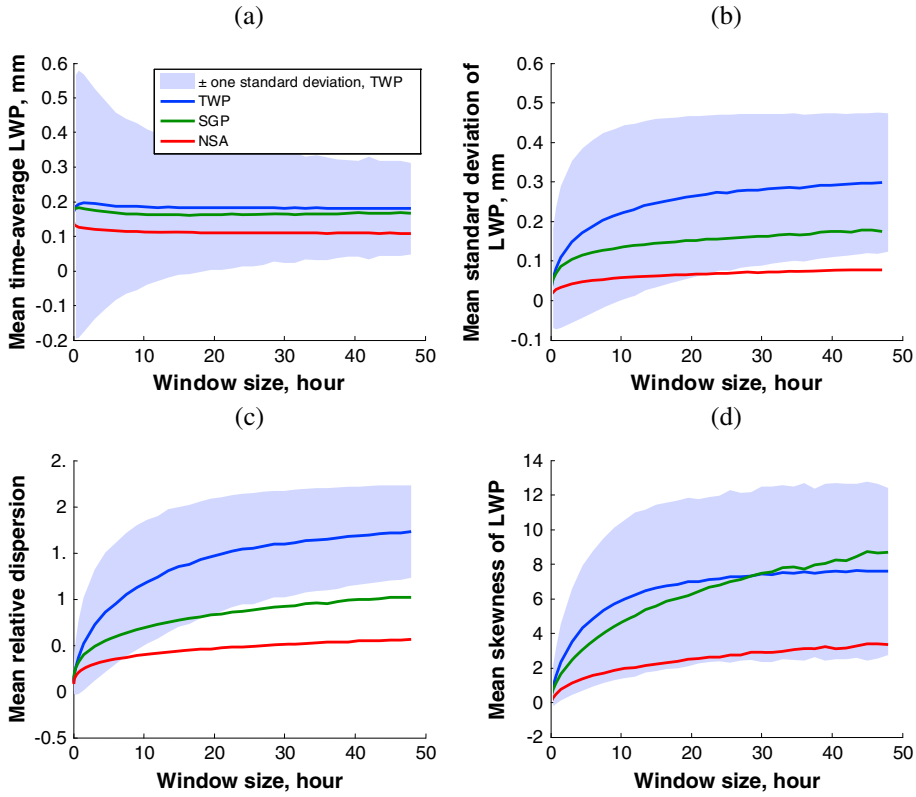

Figure 2. Scale dependence of the statistical moments of cloud LWP. The shaded area indicates the spread about the mean value at the TWP site by 1 standard deviation. (a) Mean grid-average LWP, (b) mean standard deviation, (c) mean relative dispersion, and (d) mean skewness.

the lowest LWP. The shaded area indicates the spread (1 standard deviation) of the time-average LWPs at the TWP site (the spreads of LWP at the other two sites are similar and not shown here). The spread is about 0.38 mm for very small window sizes, and it gradually decreases to 0.18 mm when the window size exceeds 20 h. Note that the definition of standard deviation used here is different with that used in the rest of the sections of this paper: the standard deviation (or the spread) of the time-average LWP describes the spread in the time-average LWP values from the entire period, while the standard deviation used in the rest of this paper is calculated for the 20 s LWP retrievals within each averaging window.

For all the three sites, the mean standard deviation is close to zero when the window size is very small ($<$10 min), and it rises sharply with increasing window size (Figures 2b). However, this result does not necessarily imply that cloud variability will vanish when the window is small, since the microwave radiometer measurements are smoothed by the relatively wide beam (4 to 6°) of the radiometer. To infer subminute cloud variability, narrow field of view sensors such as the cloud radar should be used. When the window increases to larger than 12 h, the mean standard deviation almost levels off and approaches a constant value (0.3 mm at the TWP site, 0.16 mm at the SGP site, and 0.05 mm at the NSA site). Throughout the range of the examined window sizes, the mean standard deviation at the TWP site is largest and that at the NSA site is smallest. Similar behaviors have been found using satellite-based cloud retrieval data [*Hill et al.*, 2012]. The spread of the standard deviation of LWPs at the TWP site is almost constant throughout the examined window sizes (indicated by the shaded area).

It has been reported in literature that there is a positive relationship between the mean and the standard deviation of cloud condensate [*Barker et al.*, 1996; *Boutle et al.*, 2013]. To account for this correlation, a nondimensional parameter, the ratio of standard deviation to mean cloud water content (or the inverse of this ratio), has been proposed to use in the parameterizations of subgrid cloud heterogeneity [*Shonk et al.*, 2010; *Boutle et al.*, 2013; *Oreopoulos and Davies*, 1998]. This ratio has also been widely used in statistical analysis to characterize the PDF width in the name of coefficient of variation and in cloud physics to measure

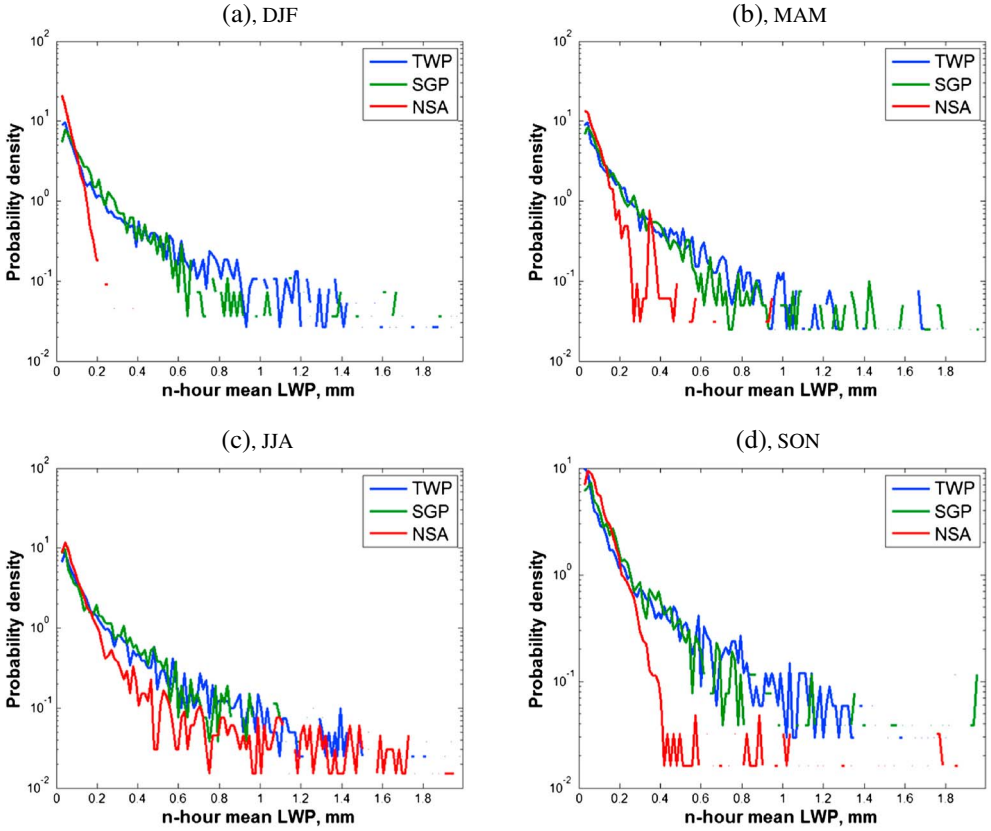

Figure 3. Seasonal variation of the *n*-hour mean cloud LWP distribution at the TWP, SGP, and NSA sites during the period of 1999–2012. The windows size *n* is chosen to be 5.0, 3.0, and 3.3 h for the three sites based on the typical wind speed at each site. (a) December, January, and February (DJF); (b) March, April, and May (MAM); (c) June, July, and August; and (d) September, October, and November. The *y* axis is the probability density normalized to have unit area under each curve.

the relative width of droplet size distributions in the name of relative dispersion [*Liu and Daum*, 2000]. Throughout this study, this ratio is referred to as relative dispersion. The mean relative dispersion shows similar dependence on window size as that of the mean standard deviation (Figure 2c): it rises from a close to zero value ($<$0.1) to about 1.6 at the TWP site, 0.8 at the SGP site, and 0.4 at the NSA site when the window size increases from a few minutes to 2 days. It is evident that the mean relative dispersion keeps increasing with increasing window size, but the slope of curve becomes less steep for larger window sizes. The mean relative dispersion at the TWP site is higher than that at the other two sites, and the NSA sites has the smallest relative dispersion across all the examined window sizes.

In all the three sites, the mean skewness of LWP is close to zero when the window size is very small (Figure 2d), indicating that the distribution of LWP, on average, is almost symmetric in a small time window. The skewness for individual time window fluctuates a lot and can take either positive or negative values. At the TWP site, the mean skewness first increases quickly with window size then almost levels off when the time window reaches 12 h. At the SGP and NSA sites, the increasing rate of mean skewness with increasing window sizes also decreases with window size, and the curve does not completely level off even when the time window is larger than 1 day. Among the three sites, the NSA site has the smallest skewness across all the examined window sizes. The distributions of cloud LWP at the TWP and SGP sites are highly positively skewed for large window sizes: the mean skewness exceeds 5 when the window size is larger than 1 day.

4. Statistical Moments of Cloud LWP in Current GCM Grid

After examining the scale dependence of the statistical moments of cloud LWP, this section focuses on a more detailed analysis of the statistical moments at the scale of a typical GCM grid, i.e., the frequency distribution of these moments. The typical gridbox size of current climate models is ~100 km, corresponding to a 3 h time

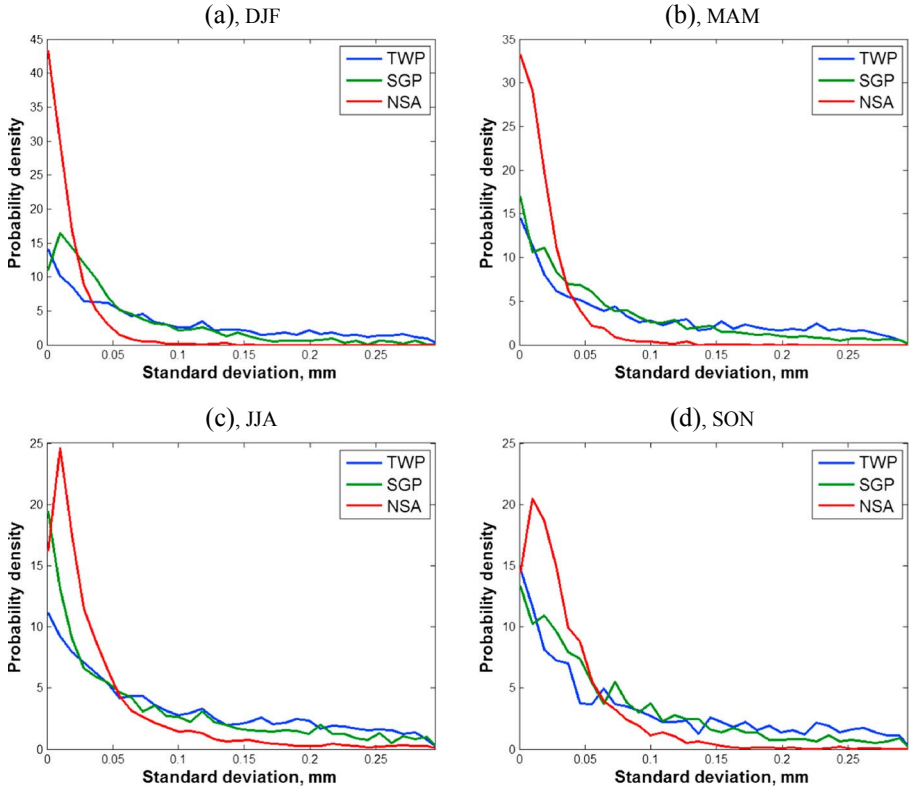

Figure 4. Seasonal variation of the standard deviation of cloud LWP calculated in *n*-hour windows at the TWP, SGP, and NSA sites during the period of 1999–2012. The windows size *n* is chosen to be 5.0, 3.0, and 3.3 h for the three sites based on the typical wind speed at each site. (a) December, January, and February (DJF); (b) March, April, and May (MAM); (c) June, July, and August; and (d) September, October, and November.

window if a mean wind speed of 10 m/s is assumed. Using the radiosonde-based wind measurements from the ARM Program [*Xie et al.*, 2010], we estimate that the mean horizontal wind speeds at typical liquid cloud base height are about 6.0, 10, and 9.0 m/s at the TWP, SGP, and NSA sites. Therefore, the averaging windows size *n* is chosen to be 5.0, 3.0, and 3.3 h for the three sites. For convenience, the term *n* hour thereinafter implies 5.0, 3.0, and 3.3 h for the TWP, SGP, and NSA sites, respectively. The statistical moments, i.e., mean, standard deviation, relative dispersion, and skewness, are first calculated for each *n*-hour averaging window using the data from 1999 to 2012. Let *q* be a statistical moment of the observed cloud LWP; the discretized PDF of this observed moments can be obtained using equation (1):

$$P(q) = \frac{n(q_i \le q < q_{i+1})}{(q_{i+1} - q_i)N} \tag{1}$$

where *N* is the total number of moment values and $n(q)$ is the number of moment values falling between q_i and q_{i+1}. The bin sizes of the discretized PDFs for the mean, standard deviation, relative dispersion, and skewness of LWP are 0.005 mm, 0.005 mm, 0.05, and 0.1, respectively. We examined the effects of choosing different bin size for the derived PDFs, and it appears that the shape of the PDF is largely insensitive to the bin size.

4.1. The *n*-Hour Mean Cloud Water Path

Figure 3 shows the PDFs of *n*-hour mean LWP at the TWP, SGP, and NSA sites for each season during the period of 1999 to 2012. Spring, summer, autumn, and winter, respectively, correspond to MAM (March, April, and May); June, July, and August; September, October, and November; and DJF (December, January, and February). The probability density of *n*-hour mean LWP peaks at a very small value. At the TWP and SGP sites, the probability density decreases very quickly to about 10% of the maximum value when the mean LWP exceeds 0.2 mm for all the four seasons. At the NSA site, the mean LWP at which the probability density decreases to about 10% of the maximum value is about 0.2 mm for summer and autumn and 0.1 mm for winter and spring. It can be seen

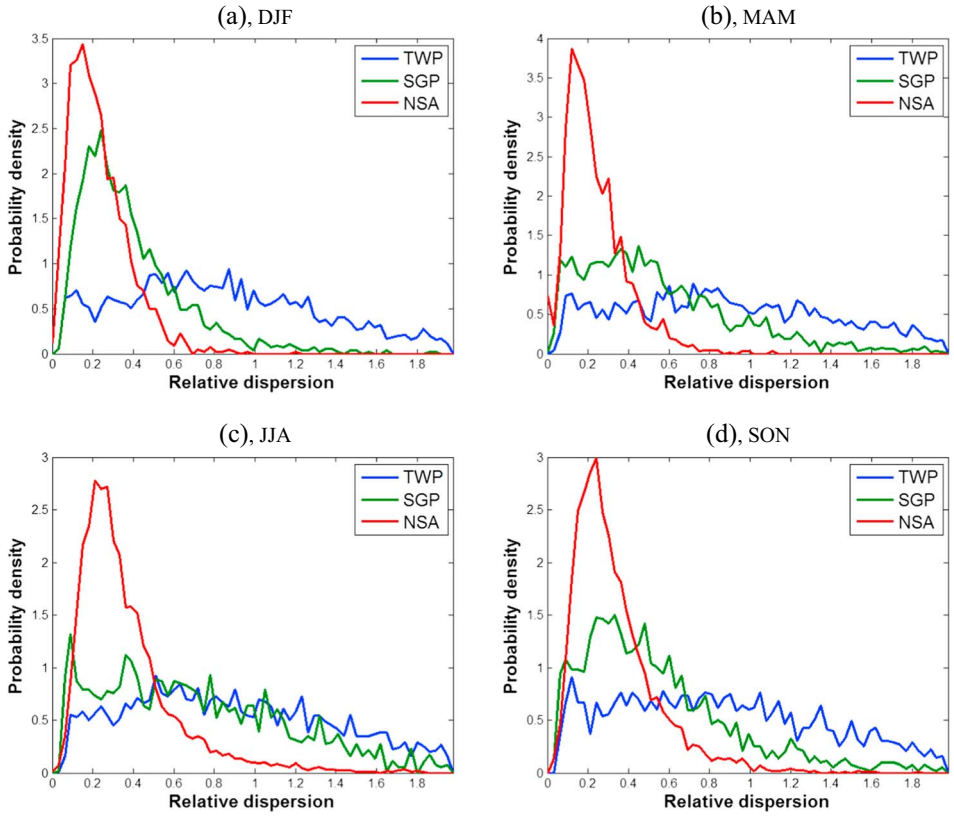

Figure 5. Seasonal variation of the relative dispersion of cloud LWP calculated in *n*-hour windows at the TWP, SGP, and NSA sites during the period of 1999–2012. The windows size *n* is chosen to be 5.0, 3.0, and 3.3 h for the three sites based on the typical wind speed at each site. (a) December, January, and February (DJF); (b) March, April, and May (MAM); (c) June, July, and August; and (d) September, October, and November.

that at all the three sites, the distributions have long tails; therefore, the distributions are positively skewed. The LWP PDFs at the TWP and SGP sites have almost identical shape in all four seasons; the tail of the distribution is slightly more significant in the summer season. In summer, similar to the other two sites, the LWP distribution at the NSA site also has a noticeable tail, but in the other seasons, the NSA site has much less frequent occurrence of large LWP values than the other two sites, and the slope of probability-LWP curve is much steeper.

4.2. Standard Deviation of Cloud Water Path

While the mean cloud condensate has been widely used in GCM cloud representations, the variance of cloud condensate is often neglected or only considered by an implicit assumption lurking in relevant parameterization schemes. Figure 4 shows the seasonal PDFs of the standard deviation of cloud LWP calculated in each *n*-hour averaging window at the TWP, SGP, and NSA sites. The annual mean standard deviations at the TWP and SGP sites have similar magnitudes, being, respectively, 0.15 and 0.12 mm, while the NSA site has a much smaller mean standard deviation (0.04 mm). There is considerable variation of seasonal mean standard deviation at the SGP and NSA sites: the summer season has the largest standard deviation (0.13 and 0.022 mm at the SGP and NSA sites), and the winter season has the lowest standard deviation (0.090 and 0.018 g m^{-2} at the SGP and NSA sites). The shape of the standard deviation distribution is to some extent similar to that of the *n*-hour mean LWP. The probability density peaks at standard deviation values smaller than 0.01 mm and monotonically decreases with increasing standard deviation value. The distribution of standard deviation at the TWP site has a slightly heavier tail than that at the SGP site, while the NSA site has noticeably fewer occurrences of large standard deviation values.

4.3. Relative Dispersion of Cloud LWP

The distributions of relative dispersion calculated in each *n*-hour averaging window at the three ARM sites are shown in Figure 5. The annual mean relative dispersions at the TWP, SGP, and NSA sites are, respectively, 0.73,

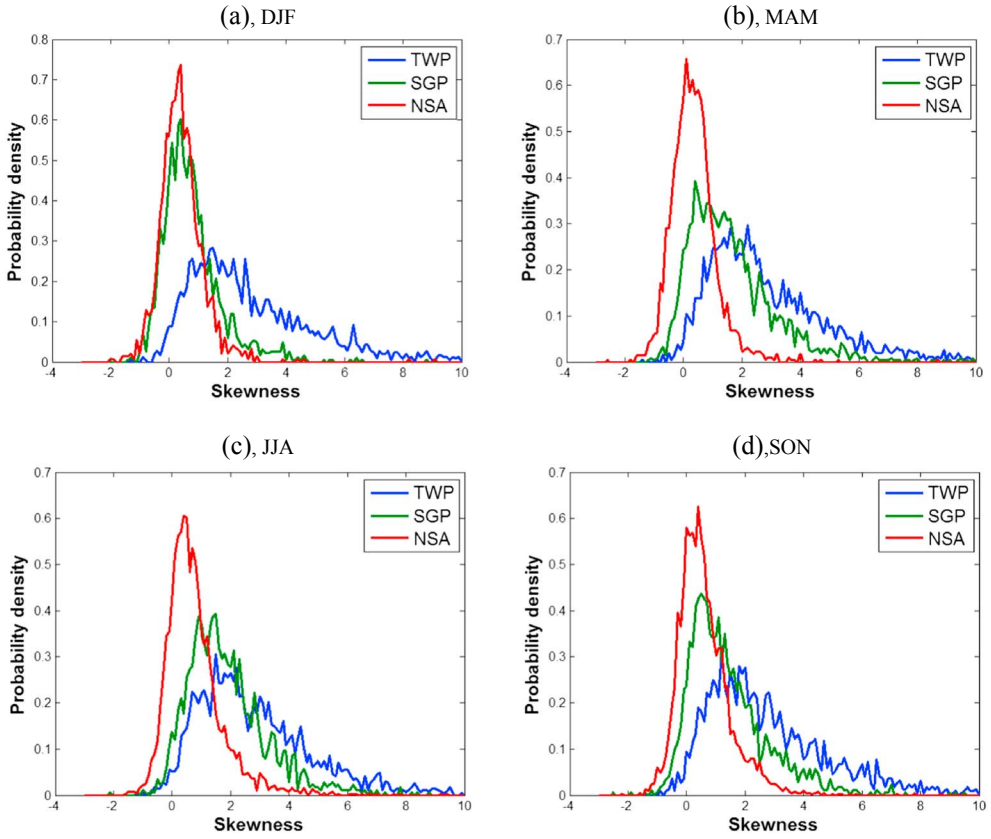

Figure 6. Seasonal variation of the skewness of cloud LWP calculated in *n*-hour windows at the TWP, SGP, and NSA sites during the period 1999–2012. The windows size *n* is chosen to be 5.0, 3.0, and 3.3 h for the three sites based on the typical wind speed at each site. (a) December, January, and February (DJF); (b) March, April, and May (MAM); (c) June, July, and August; and (d) September, October, and November.

0.50, and 0.33; these values are lower than those suggested by satellite-based optical thickness observations [*Barker et al.*, 1996]. It should be noted that *Barker et al.* [1996] expresses cloud variability in terms of cloud optical depth, which is a function of both cloud condensate mass and cloud droplet effective radius. The mean relative dispersion values at the three sites are also lower than those used in some GCM cloud subgrid variability parameterizations [*Morrison and Gettelman*, 2008]. The probability density decreases much faster with increasing relative dispersion value at the NSA site than at the other two sites, resulting in a less tailed distribution at the NSA site.

Similar to the standard deviation, the SGP and NSA sites show considerable seasonal variation of relative dispersion. The distributions of relative dispersion have the most noticeable tail in summer, with the mean relative dispersion being 0.57 and 0.26 at the SGP and NSA sites, respectively. The mean relative dispersion is 0.40 and 0.22 at these two sites.

4.4. The Skewness of Cloud LWP

Similar to the relative dispersion, skewness is also a nondimensional statistical property of a distribution. Figure 6 shows the PDF of skewness of LWP calculated in *n*-hour windows for each season at the three ARM sites using the data from the period of 1999 to 2012. The annual mean LWP skewness values are, respectively, 2.6, 1.5, and 0.6 at the TWP, SGP, and NSA sites, which confirm the findings in previous studies that the distributions of LWP have heavy positive tails [*Barker et al.*, 1996]. The LWP at the NSA site has the smaller skewness, possibly due to the dominance of stratus clouds over the arctic area, while the tropical site, where deep convection cloud systems are often found in this "warm pool" region, has the largest mean skewness. All of the three distributions show evident modals, peaking, respectively, at 0.9, 0.4, and 0.2. The peak of the skewness distribution seems to shift toward larger values when moving from the NSA, to the SGP, and to the TWP sites. Accompanying this shift, the distribution is getting wider and more positively skewed as moving

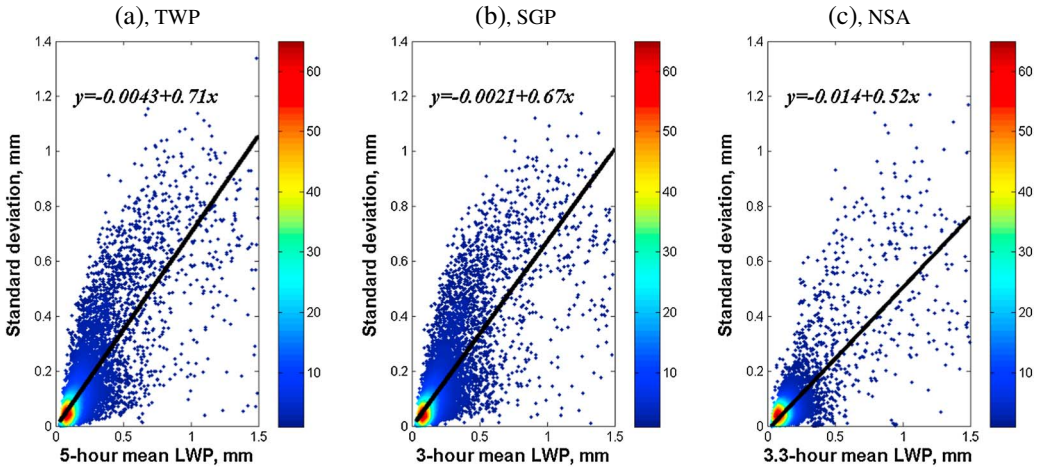

Figure 7. Scatterplot of *n*-hour mean LWP and standard deviation at the (a) TWP, (b) SGP, and (c) NSA sites for the period of 1999 to 2012. The corresponding linear regressions are shown as the black lines.

from the arctic site to the tropic site. About 2% of the cloudy cases at the NSA site have a skewness larger than 3, while the TWP and SGP sites, respectively, have more than 20% of the cases with a skewness larger than 3.

The SGP and NSA sites show similar seasonal variation of skewness as relative dispersion and standard deviation, while the TWP site has much smaller seasonal variation. The mean skewness is, respectively, 1.7 and 0.43 at the SGP and NSA sites in summer and 0.85 and 0.40 at these two sites in winter.

5. Relationship Between the Moments

As shown in several studies [*Tompkins*, 2002; *Golaz et al*., 2002], it is possible to derive prognostic equations for high-order statistical moments of cloud properties based on high-order turbulence closure schemes. Phenomenal relationships between high-order moments and low-order moments based on observational and modeling studies can be used to provide diagnostic constraints for the high-order moments. This section examines the relationship between the various statistical moments.

The scatterplot of the *n*-hour mean and standard deviation of cloud LWP at each site is shown in Figure 7. The linear regression line is indicated as a black line on each plot. It can be seen that the standard deviation is positively correlated with the mean LWP with a correlation coefficient (*R* value) of about 0.8, but the relationship is largely scattered. This is consistent with the findings in previous observational studies [*Kim et al*., 2005]. The slope of the linear regression line of standard deviation (σ) versus *n*-hour mean LWP ($\overline{q}$) ranges from 0.52 to 0.71 for the three sites, and the uncertainty of the estimated slope is less than 0.01. The intercept of each regression line is negligible. The regression derived that used all data from the sites is

$$\sigma = -0.0050 + 0.66\overline{q} \tag{2}$$

Using the fixed relationship (equation (2)) to approximate the standard deviation of cloud LWP in terms of mean LWP will result in a mean error of less than 8% in each site. For all of the three sites, the positive relationship becomes less evident with increasing LWP. A decreasing trend becomes evident when LWP exceeds 0.9 mm. The decreasing trend can be explained by the fact that large mean LWP values are more likely to be related with overcast sky conditions with a smaller magnitude of variability than partially cloudy conditions [*Hill et al*., 2012; *Wood and Hartmann*, 2006].

Figure 8 shows the scatterplot of the *n*-hour relative dispersion and mean LWP at the three sites. It can be seen that there is no well-defined relationship between these two quantities at all three sites. The relative dispersion fluctuates dramatically between 0 and 3.8 at small LWP values where the sensitivity to LWP is highest. The variability of relative dispersion decreases with increasing mean LWP and centers around about 0.5 when LWP exceeds 0.8 mm. The collapse of the linear relationship between mean LWP and standard deviation at high LWP values (Figure 7) as well as the large variability of relative dispersion indicate that it is more appropriate to parameterize the relative dispersion as a function of mean LWP than to use a fixed relative dispersion value in GCMs [*Morrison and Gettelman*, 2008].

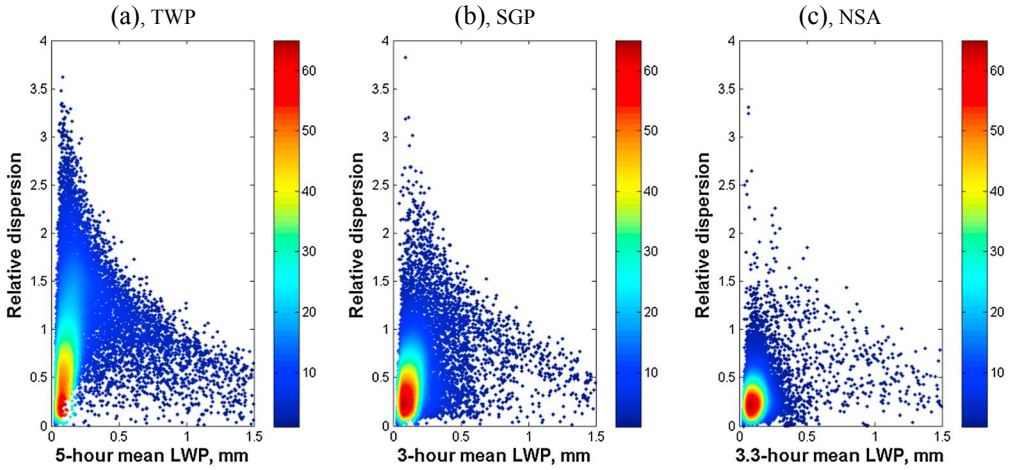

Figure 8. Scatterplot of *n*-hour mean LWP and relative dispersion at the (a) TWP, (b) SGP, and (c) NSA sites for the period of 1999 to 2012.

The scatterplot of skewness versus mean LWP (Figure 9) appears to have a similar shape as that of relative dispersion versus mean LWP. There is no meaningful correlation between these two quantities at all three sites. For small LWP, the skewness has large variation ranging from -2 to almost 10. The TWP site has more cases with high skewness and low LWP than the other two sites. The range of variation of skewness quickly shrinks with increasing LWP value. The skewness remains almost constant and fluctuates only slightly around 0.5 when the mean LWP exceeds 0.5 mm.

Figure 10 further explores the relationship between skewness and relative dispersion. It can be seen that there is a positive correlation between the observed skewness and the relative dispersion at all three sites. A linear regression line forced to have a zero intercept is overlaid on each scatterplot, since the skewness should be close to zero if the relative dispersion is small. The data points are mostly clustered within the region of relative dispersion < 1.0 and skewness < 3.0. The slope is, respectively, 2.65, 2.34, and 2.17 for the TWP, SGP, and NSA sites, and the uncertainty of the estimated slope is less than 0.03. The linear regression equation based on the data from all three sites is

$$S = 2.43\varepsilon \tag{3}$$

where S and ε represent the skewness and the relative dispersion. Again, the uncertainty of the estimated coefficient is about 1%. The correlation coefficient value is about 0.6. Although the slope of skewness versus relative dispersion at each site is statistically different, using equation (3) will result in an error of less than 10%.

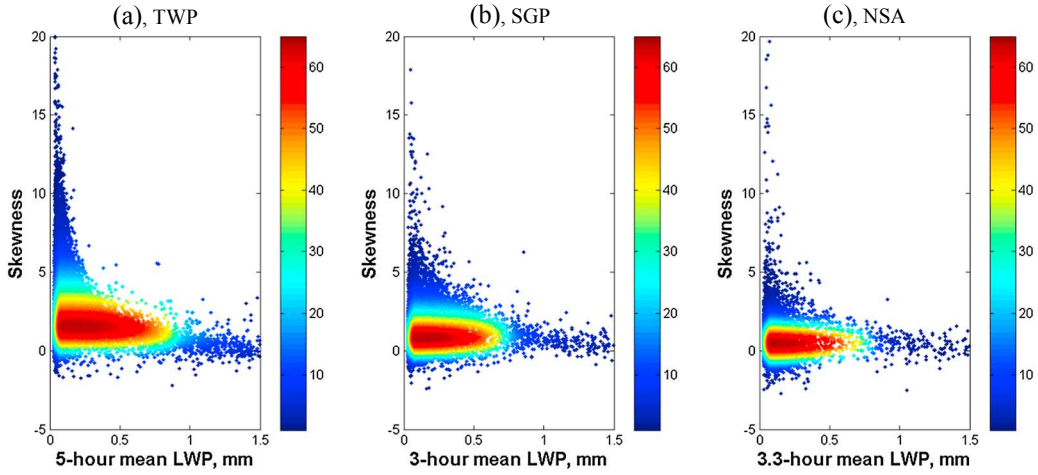

Figure 9. Scatterplot of the *n*-hour mean LWP and skewness at the (a) TWP, (b) SGP, and (c) NSA sites for the period of 1999 to 2012.

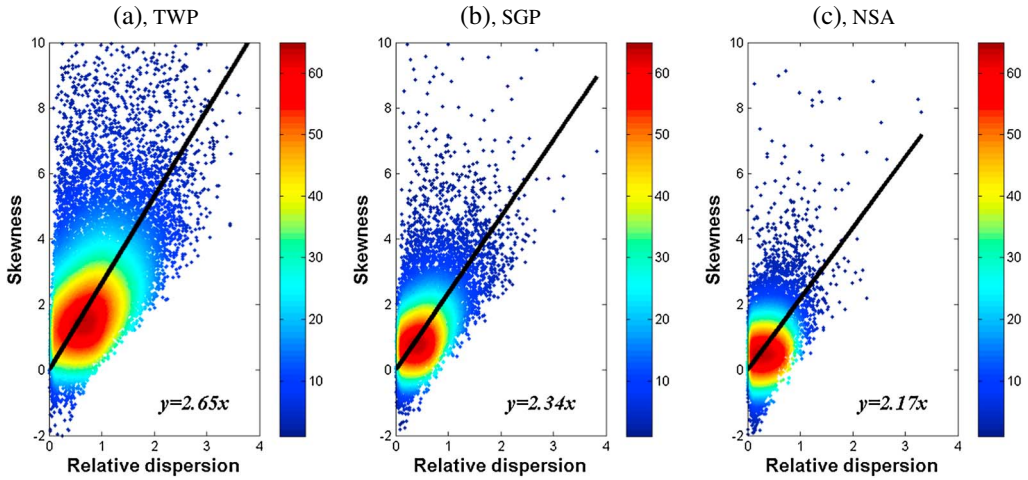

Figure 10. Scatterplot of skewness and relative dispersion of LWP calculated in *n*-hour windows at the (a) TWP, (b) SGP, and (c) NSA sites. The linear regression lines are forced to have zero intercept.

6. PDFs of Cloud LWP

Sections 3–5 explore the scale dependence, probability distribution of the statistical moments of cloud LWP, and the relationship between these moments. The moments are commonly used to determine the parameters of assumed distribution functions of subgrid cloud condensate. To shed light on which distribution function is optimal for representing subgrid cloud variability, this section examines which of the commonly used distribution functions is able to produce consistent results as the observed relationship between the statistical moments. Specifically, four distribution functions are examined: truncated Gaussian, gamma, lognormal, and Weibull. Section A1 provides some general description of these distribution functions. The truncated Gaussian distribution is chosen to be the nonnegative portion of a symmetric Gaussian distribution; thus, the skewness of a truncated Gaussian is always nonnegative. The gamma and lognormal distributions are also positively skewed. Depending on the choice of the shape parameter, the Weibull distribution can be either positively or negatively skewed.

6.1. PDFs of Climatological Cloud LWP

We first use equation (1) with q = LWP to obtain the observed PDF of cloud LWP at the TWP, SGP, and NSA sites for the period of 1999 to 2012. Figure 11 shows the observed PDFs of cloud LWP at the three ARM sites. The observed distributions of LWP are all positively skewed with the most probable LWP being smaller than 0.05 mm. The PDF of cloud LWP quickly decreases with increasing LWP. For the TWP site, the probability density of LWP = 0.1 mm drops to less than 10% of its maximum value. The PDF of LWP at the SGP site decreases slower with increasing LWP for LWP $<$ 0.07 mm but much quicker for LWP $>$ 0.1 mm than at the TWP site (Figure 11, the logarithm plot). For the NSA site, the PDF of LWP decreases to 10% and 1% of the maximum value at LWP = 0.2 mm and LWP = 0.4 mm, respectively.

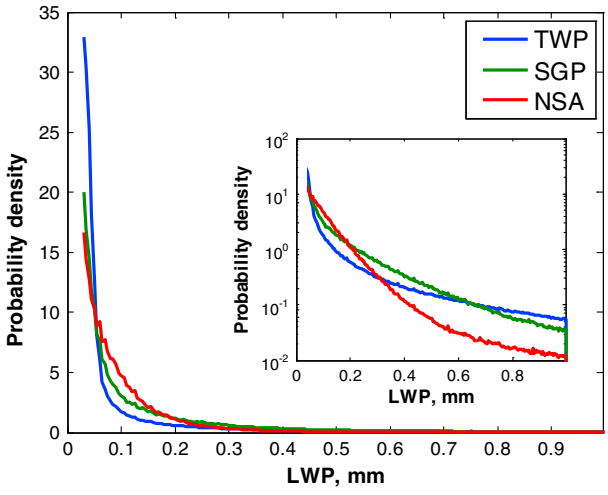

Figure 11. The observed PDFs of 20 s cloud LWP at ARM's TWP, SGP, and NSA sites for the period of 1999 to 2012.

The observed PDFs of cloud LWP are then approximated by the Gaussian, gamma, lognormal, and Weibull distribution functions using a moment-preserving approach. The moment approach tries to find optimal

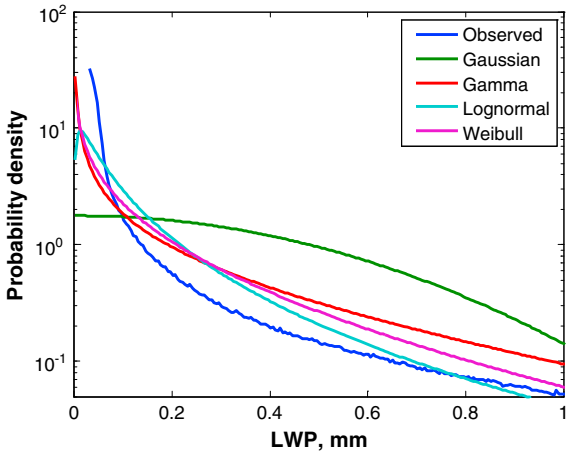

Figure 12. The parameterized PDFs of climatological cloud LWP at the TWP site derived using the moment approach.

distribution parameters for each distribution function that produces the same first and second statistical moments as the original distributions. More details on how to apply the moment approach for each distribution function are provided in section A2. Figure 12 compares the observed PDF of cloud LWP at the TWP site during the same 14 year period with the derived Gaussian, gamma, lognormal, and Weibull distribution functions using the moment approach. It is clear that all of the derived distributions underestimate the very left part of the observed distribution where the frequency of occurrence is highest but largely overestimate the right tail of LWP distribution. The Gaussian distribution function fails to capture the shape of the observed distribution and appears to largely overestimate the tail. The derived gamma distribution is similar to the Weibull distribution across the entire range of LWP. The lognormal distribution appears to better approximate the right tail of the observed distribution than the gamma and Weibull distributions.

6.2. PDFs of Subgrid Cloud LWP

We use the same approach as that used in section 6.1 to derive distribution functions for each *n*-hour window at each site. To judge which distribution function better approximate the observed subgrid-scale distribution of cloud LWP, one could use popular goodness of fit tests, including the Kolmogorov–Smirnov, Anderson–Darling, and chi-square tests [*Kolmogorov*, 1941; *Anderson and Darling*, 1952]. These goodness of fit tests typically measure the "distance" between the data and the distribution being tested and compare that distance to the critical value. In the climate system, many processes such as cloud microphysical and radiative transfer processes differently respond to different portion of the cloud condensate distribution because of their nonlinear relationships with cloud condensate. Therefore, these widely used goodness of fit tests may not be the best tools for telling whether a specific distribution function is able to produce accurate grid-average microphysical or radiative process rates. Furthermore, these tests measure the goodness of fit for individual functions/curves, not how good a family of distribution functions with different distribution parameters compare with observations. Thus, this study focuses on testing whether the commonly used distribution functions are able to produce similar relationship between the nondimensional moments as that derived from observations and follows an approach similar to that used to identify the best function to describe the pattern of observed droplet size distributions [*Liu and Daum*, 2000].

For gamma and lognormal distributions, the relative dispersion and skewness are, respectively, related to each other by equations (4) and (5):

$$S = 2\varepsilon, \quad \text{for gamma distributions} \tag{4}$$

$$S = 3\varepsilon + \varepsilon^3, \quad \text{for lognormal distributions} \tag{5}$$

For the truncated Gaussian and Weibull distributions, the relative dispersion and skewness are also uniquely related to each other in a closed form, although the relationships cannot be expressed in simple analytical forms.

The theoretical relationships between skewness and relative dispersion for the truncated Gaussian, gamma, lognormal, and Weibull distributions are shown together with the scatterplot of 3 h skewness and relative dispersion in Figure 13. It can be seen that the truncated Gaussian distribution at best poorly produces the observed relationship between skewness and relative dispersion when the relative dispersion is small (relative dispersion < 0.3) and significantly underestimates the skewness for relative dispersion > 0.5. Another property of the truncated Gaussian distribution is that it cannot produce skewness values larger than one no matter what parameters are chosen to specify the distribution. The gamma and lognormal distributions allow only positive skewness, while negative skewness is also found in observations. The Weibull distribution

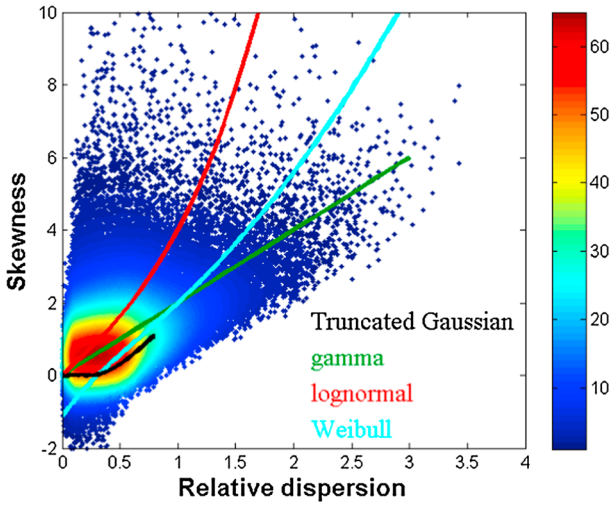

Figure 13. The scatterplot of the skewness and the relative dispersion of LWP calculated in *n*-hour windows using the data from all the three sites for the period of 1999 to 2002. The color in the scatterplot indicates the density of data points. The theoretical curves of the truncated Gaussian, gamma, lognormal, and Weibull distributions are also shown.

permits both positive and negative skewness and seems to follow the observations reasonably well in the examined range of relative dispersion. The skewness-dispersion curves of the gamma, lognormal, and Weibull distributions start to diverge after the relative dispersion exceeds 0.5: the lognormal and Weibull curves seem to stay with the bulk of the scatterplot, while the gamma curve passes through the lower portion of the scatterplot.

To further evaluate the four distribution functions, we introduce a quantitative measure defined as the shortest distance of each data point in the scatterplot to the theoretical curves. A small distance suggests a better fitting of the corresponding distribution function. Figure 14 shows the mean shortest distance for each distribution function as a function of relative dispersion; the mean shortest distance is calculated as the average of distances from the data points to the theoretical curves. A few points are worth noting. First, the mean shortest distance to the curves increases with increasing relative dispersion values. Second, the truncated Gaussian distribution results in the largest distance over the whole range of relative dispersion. The lognormal distribution clearly outperforms the other three distributions when relative dispersion < 1.0, and this is consistent with Figure 13. For relative dispersion > 1.5, the mean shortest distance of the lognormal distribution is significantly larger than those of the Weibull and gamma distributions but much smaller than that of the truncated Gaussian distribution. Overall, it appears that the three heavily tailed distributions, i.e., Weibull, Gamma, and lognormal distributions, all reproduce the observed relationship between skewness and relative dispersion reasonably well. The mean shortest distances are 2.2, 0.46, 0.43, and 0.69 for the truncated Gaussian, Weibull, gamma, and lognormal distribution functions, respectively.

It is noteworthy that we have examined the PDFs over a wide range of gridbox sizes from 50 min to 6 h and found similar results: the lognormal and gamma distributions best represent the relationship between skewness and relative dispersion.

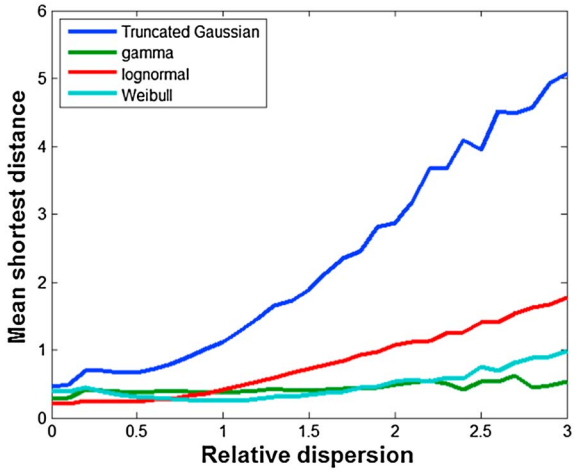

Figure 14. The mean shortest distance of data points to each theoretical curve in Figure 13 as a function of relative dispersion.

7. Summary

We use the 14 year long LWP retrieval data from the TWP (tropical), SGP (midlatitude), and NSA (arctic) sites of the DOE ARM Program to examine the statistical characteristics of cloud spatial variability. We first examine the dependence of four statistical moments on scale (i.e., gridbox size or averaging window size). The statistical moments examined in this study include the mean, standard deviation, relative dispersion (defined as the ratio of the standard deviation to the mean), and skewness. It is found that the mean LWP does not vary with gridbox size. The standard deviation, relative dispersion, and skewness monotonically increase with gridbox size, while the increasing rate decreases with increasing gridbox size.

We then take a close look at the PDFs of the four moments calculated in *n*-hour windows (roughly corresponds to the gridbox size of present GCMs). There is considerable seasonal variation of the observed statistical moments of cloud LWP at the SGP and NSA sites, while the seasonal variation is much smaller at the TWP site. The PDFs of *n*-hour mean cloud LWP in all the three sites show no modal in the examined range of LWP values (0.03 mm to 3 mm), and the probability density rapidly decreases with increasing LWP. The mean *n*-hour standard deviations at the three sites are, respectively, 0.15, 0.12, and 0.04 mm. The PDFs of standard deviation peak at values smaller than 0.01 mm and monotonically decrease with increasing standard deviation value. The NSA site has smaller standard deviation than the TWP and SGP sites. The mean relative dispersions at the TWP, SGP, and NSA sites are, respectively, 0.73, 0.50, and 0.33, lower than those suggested by satellite-based optical thickness observations [*Barker et al.*, 1996] and those used in some GCM cloud subgrid variability parameterizations [*Morrison and Gettelman*, 2008]. It is evident that the PDFs of the skewness of *n*-hour LWP at the three sites have one modal; the most probable skewness values for the TWP, SGP, and NSA sites are, respectively, 0.9, 0.4, and 0.2.

The relationships between the statistical moments are also explored. There is a positive correlation between the *n*-hour mean LWP and the standard deviation with a correlation coefficient of 0.8, but the positive relationship does not hold for LWP $>$ 0.9 mm. The relative dispersion dramatically varies when LWP is small (LWP $<$ 0.3 mm) and tends to converge to around 0.5 for large LWP. There is almost no correlation between the mean LWP and the skewness. The skewness and the relative dispersion are positively correlated with an *R* value of 0.6. The skewness and relative dispersion relationship is reasonably explained by assuming that the PDF of cloud LWP in each *n*-hour window is a lognormal, Weibull, or Gamma distribution.

Lastly, we compare the theoretically expected relationship between relative dispersion and skewness for the truncated Gaussian, gamma, lognormal, and Weibull distributions with the observed relationship. The results show that constrained by the same mean and standard deviation values, the truncated Gaussian distribution is unable to produce large skewness or relative dispersion values. The Weibull distribution is the only one that can produce negative skewness that is found in observations. The theoretical curves of skewness versus relative dispersion for the gamma and lognormal distributions are similar at small relative dispersion values and start to diverge after the relative dispersion exceeds 0.5: the lognormal and Weibull curves stay in the center of the scatterplot, while the gamma curves pass through the lower portion of the scatterplot. Overall, the three heavily tailed distributions, i.e., the lognormal, Weibull, and Gamma distributions, better produce the observed relationship between skewness and relative dispersion than the truncated Gaussian distribution. However, further research is still needed to determine which distribution is the optimal choice for parameterizing cloud subgrid variability. Since the major motivation of introducing cloud subgrid variability in GCMs is to improve the parameterizations of cloud microphysical and radiative transfer processes, we will directly evaluate the accuracy of using such functions to represent subgrid cloud variability in microphysical process rate and radiative flux calculations in a companion paper.

Appendix A: Statistical Moments of Several Distribution Functions

A1. Commonly Used Distribution Functions

Four distribution functions are used to approximate the observed distribution of cloud LWP; they are truncated Gaussian, gamma, lognormal, and Weibull distributions [*Forbes et al.*, 2010].

Given the fact that cloud condensate cannot take negative values, the truncated Gaussian distribution can be expressed as

$$P(q) = \frac{e^{-\frac{(q-\mu)^2}{2s^2}}}{\sqrt{2\pi}s}/a, \text{ for } q \geq 0 \tag{A1}$$

where $a = \left[1 + \text{erf}\left(\frac{\mu}{\sqrt{2}s}\right)\right]/2$ is the normalization factor for the truncated Gaussian distribution.

The PDF of a gamma distribution is

$$P(q) = \frac{q^{k-1}e^{-q/\theta}}{\theta^k \Gamma(k)}, \text{ for } q > 0 \text{ and } k, \ \theta > 0 \tag{A2}$$

Here $\Gamma(k)$ is the gamma function, k and θ are, respectively, the shape and scale parameters of the gamma distribution.

Similarly, the lognormal distribution can be written as

$$P(q) = \frac{1}{qs\sqrt{2\pi}} e^{-\frac{(\ln q-\mu)^2}{2s^2}}, \quad \text{for } q > 0 \tag{A3}$$

The parameters μ and s are, respectively, the mean and the standard deviation of the variable's natural logarithm.

The PDF of a Weibull distribution is

$$P(q) = \frac{k}{\theta}\left(\frac{q}{\theta}\right)^{k-1} e^{-(q/\theta)^k}, \quad \text{for } q \geq 0 \text{ and } k, \theta > 0 \tag{A4}$$

Here k and θ are, respectively, the shape and scale parameters of the Weibull distribution.

A2. Determination of Distribution Parameters Based on Statistical Moments

All of the four distribution functions mentioned above can be specified using two parameters. If the first two statistical moments, i.e., the mean ($\overline{q}$) and the variance (σ^2) of cloud water, can be obtained from observations or models, then it is possible to uniquely determine the distribution parameters.

For the truncated Gaussian distribution, the first two moments can be written as

$$\begin{aligned} \overline{q} &= \frac{se^{-\mu^2/2s^2}}{\sqrt{2\pi}}/a + \frac{\mu}{2}\left[1 + \text{erf}\left(\frac{\mu}{\sqrt{2}s}\right)\right]/a \\ \sigma^2 &= \frac{\mu se^{-\mu^2/2s^2}}{\sqrt{2\pi}}/a + \frac{\mu^2 + s^2}{2}\left[1 + \text{erf}\left(\frac{\mu}{\sqrt{2}s}\right)\right]/a - \overline{q}^2 \end{aligned} \tag{A5}$$

where a is the normalization factor as mentioned in section A1 and erf is the error function.

For the gamma distribution, the shape and scaling parameters are related to the moments by

$$\begin{aligned} \overline{q} &= k\theta \\ \sigma^2 &= k\theta^2 \end{aligned} \tag{A6}$$

For the lognormal distribution, the relationship between the first two statistical moments and the lognormal parameters can be expressed as

$$\begin{aligned} \overline{q} &= e^{\mu + \frac{s^2}{2}} \\ \sigma^2 &= \left(e^{s^2} - 1\right)e^{2\mu + s^2} \end{aligned} \tag{A7}$$

For the Weibull distribution, the relationship can be written as

$$\begin{aligned} \overline{q} &= \theta\,\Gamma(1 + 1/k) \\ \sigma^2 &= \theta^2\,\Gamma(1 + 2/k) - \overline{q}^2 \end{aligned} \tag{A8}$$

The parameters of the truncated Gaussian, gamma, lognormal, and Weibull distributions can be found by, respectively, solving the equations (A5)–(A8).

Acknowledgments
This work is supported by the Climate System Modeling (ESM) via the FASTER project (www.bnl.gov/faster) and the Atmospheric Science Research programs of the U.S. Department of Energy. The data used in this study are available at http://www.arm.gov.

References

Anderson, T. W., and D. A. Darling (1952), Asymptotic theory of certain "goodnessof-fit" criteria based on stochastic processes, *Ann. Math. Stat.*, *23*(2), 193–212.

Barker, H. W., B. A. Wiellicki, and L. Parker (1996), A parameterization for computing grid-averaged solar fluxes for inhomogeneous marine boundary layer clouds. Part II: Validation using satellite data, *J. Atmos. Sci.*, *53*, 2304–2316.

Battaglia, A., P. Saavedra, T. Rose, and C. Simmer (2010), Characterization of precipitating clouds by ground-based measurements with the triple-frequency polarized microwave radiometer ADMIRARI, *J. Appl. Meteorol. Climatol.*, *49*, 394–414, doi:10.1175/2009JAMC2340.1.

Boutle, I. A., S. J. Abel, P. G. Hill, and C. J. Morcrette (2013), Spatial variability of liquid cloud and rain: Observations and microphysical effects, *Q. J. R. Meteorol. Soc.*, doi:10.1002/qj.2140.

Burghelea, T., E. Serge, and V. Steinberg (2005), Validity of the Taylor hypothesis in a random spatially smooth flow, *Phys. Fluids*, *17*, 103101, doi:10.1063/1.2077367.

Cadeddu, M. P., J. C. Liljegren, and D. D. Turner (2013), The Atmospheric radiation measurement (ARM) program network of microwave radiometers: Instrumentation, data, and retrievals, *Atmos. Meas. Tech.*, *6*, 2359–2372.

Cahalan, R. F., W. Ridgway, W. J. Wiscombe, T. L. Bell, and J. B. Snider (1994), The albedo of fractal stratocumulus clouds, *J. Atmos. Sci.*, *51*, 2434–2455.

Clothiaux, E. E., T. Ackerman, G. G. Mace, K. P. Moran, R. T. Marchand, M. Miller, and B. E. Martner (2000), Objective determination of cloud heights and radar reflectivities using a combination of active remote sensors at the ARM CART sites, *J. Appl. Meteorol.*, *39*, 645–665.

Dong, X., P. Minnis, B. Xi, S. Sun-Mack, and Y. Chen (2008), Comparison of CERES-MODIS stratus cloud properties with ground-based measurements at the DOE ARM Southern Great Plains site, *J. Geophys. Res.*, *113*, D03204, doi:10.1029/2007JD008438.

Forbes, C., M. Evans, N. Hastings, and B. Peacock (2010), *Statistical Distributions*, 4th ed., John Wiley, Hoboken, N. J., doi:10.1002/9780470627242.ch44.

Golaz, J.-C., V. E. Larson, and W. R. Cotton (2002), A PDF-based model for boundary layer clouds. Part I: Method and model description, *J. Atmos. Sci.*, *59*, 3540–3551.

Griffin, B. M., and V. E. Larson (2013), Analytic upscaling of local microphysics parameterizations. Part II: Simulations, *Q. J. R. Meteorol. Soc.*, *139*, 58–69.

Hill, P. G., R. J. Hogan, J. Manners, and J. C. Petch (2012), Parametrizing the horizontal inhomogeneity of ice water content using CloudSat data products, *Q. J. R. Meteorol. Soc.*, *138*, 1784–1793.

Huang, D., and Y. Liu (2014), Statistical characteristics of cloud variability. Part 2: Implication for parameterizations of microphysical and radiative transfer processes in climatemodels, *J. Geophys. Res. Atmos.*, *119*, 10,829–10,843, doi:10.1002/2014JD022003.

Huang, D., Y. Liu, and W. Wiscombe (2008), Determination of cloud liquid water distribution using 3D cloud tomography, *J. Geophys. Res.*, *113*, D13201, doi:10.1029/2007JD009133.

Kain, J. S. (2004), The Kain–Fritsch convective parameterization: An Update, *J. Appl. Meteorol.*, *43*, 170–181.

Kain, J. S., and J. M. Fritsch (1990), A one-dimensional entraining/detraining plume model and its application in convective parameterization, *J. Atmos. Sci.*, *47*, 2784–2802.

Kim, B.-G., S. A. Klein, and J. R. Norris (2005), Continental liquid water cloud variability and its parameterization using Atmospheric Radiation Measurement data, *J. Geophys. Res.*, *110*, D15S08, doi:10.1029/2004JD005122.

Kneifel, S., S. Crewell, U. Löhnert, and J. Schween (2009), Investigating water vapor variability by ground-based microwave radiometry: Evaluation using airborne observations, *IEEE Geosci. Remote Sens. Lett.*, *6*(1), 157–161, doi:10.1109/LGRS.2008.2007659.

Kneifel, S., S. Redl, E. Orlandi, U. Löhnert, M. P. Cadeddu, D. D. Turner, and M. Chen (2014), Absorption properties of supercooled liquid water between 31 and 225 GHz: Evaluation of absorption models using ground-based observations, *J. Appl. Meteorol. Climatol.*, *53*, 1028–1045.

Kolmogorov, A. (1941), Confidence limits for an unknown distribution function, *Ann. Math. Stat.*, *12*(4), 461–463.

Larson, V. E., and B. M. Griffin (2012), Analytic upscaling of local microphysics parameterizations. Part I: Theory, *Q. J. R. Meteorol. Soc.*, *139*, 46–57.

Larson, V. E., R. Wood, P. R. Field, J.-C. Golaz, T. H. Vonder Haar, and W. R. Cotton (2001), Systematic biases in the microphysics and thermodynamics of numerical models that ignore subgrid variability, *J. Atmos. Sci.*, *58*, 1117–1128.

Liljegren, J., E. Clothiaux, G. Mace, S. Kato, and X. Dong (2001), A new retrieval for cloud liquid water path using a ground-based microwave radiometer and measurements of cloud temperature, *J. Geophys. Res.*, *106*, 14,485–14,500, doi:10.1029/2000JD900817.

Liu, Y., and P. H. Daum (2000), Which size distribution function to use for studies related to effective radius, Proceedings of the 13th International Conf. on Clouds and Precipitation, Reno, NV, 14-18 August, 586-589.

Minnis, P., et al. (2011), CERES Edition-2 cloud property retrievals using TRMM VIRS and Terra and Aqua MODIS data, Part I: Algorithms, *IEEE Trans. Geosci. Remote Sens.*, *49*(11), 4374–4400, doi:10.1109/TGRS.2011.2144601.

Morris, V. R. (2006), Microwave radiometer handbook. [Available at http://www.arm.gov/publications/tech_reports/handbooks/mwr_handbook.pdf?id=97.]

Morrison, H., and A. Gettelman (2008), A new two-moment bulk stratiform cloud microphysics scheme in the community atmosphere model, version 3 (CAM3). Part I: Description and numerical tests, *J. Clim.*, *21*, 3642–3659.

Oreopoulos, L., and R. Davies (1998), Plane parallel albedo biases from satellite observations. Part II: Parameterizations for bias removal, *J. Clim.*, *11*, 933–944.

Pincus, R., and S. A. Klein (2000), Unresolved spatial variability and microphysical process rates in large-scale models, *J. Geophys. Res.*, *105*, 27,059–27,065, doi:10.1029/2000JD900504.

Pincus, R., H. W. Barker, and J.-J. Morcrette (2003), A fast, flexible, approximate technique for computing radiative transfer in inhomogeneous cloud fields, *J. Geophys. Res.*, *108*(D13), 4376, doi:10.1029/2002JD003322.

Powell, D. C., and C. E. Elderkin (1974), An investigation of the application of Taylor's hypothesis to atmospheric boundary layer turbulence, *J. Atmos. Sci.*, *31*, 990–1002.

Schween, J. H., S. Crewell, and U. Löhnert (2011), Horizontal-humidity gradient from one single-scanning microwave radiometer, *IEEE Geosci. Remote Sens.*, *8*, 336–340.

Shonk, J. K. P., R. J. Hogan, G. G. Mace, and J. M. Edwards (2010), Effect of improving representation of horizontal and vertical cloud structure on the Earth's radiation budget. Part I: Review and parameterisation, *Q. J. R. Meteorol. Soc.*, *136*, 1191–1204.

Shupe, M. D., J. S. Daniels, G. de Boer, E. W. Eloranta, P. Kollias, C. N. Long, E. P. Luke, D. D. Turner, and J. Verlinde (2008), A focus on mixed-phase clouds: The status of ground-based observational methods, *Bull. Am. Meteorol. Soc.*, *89*, 1549–1562.

Stokes, M. G., and S. E. Schwartz (1994), The Atmospheric Radiation Measurement (ARM) Program: Programmatic background and design of the cloud and radiation test bed, *Bull. Am. Meteorol. Soc.*, *75*, 1201–1221.

Sun, C.-H., and L. R. Thorne (1995), Inferring spatial cloud statistics from limited field-of-view, zenith observations, in Proceedings of Fifth Atmospheric Radiation Measure (ARM) Science Team Meeting, pp. 331–334, San Diego, Calif.

Taylor, G. I. (1938), The spectrum of turbulence, *Proc. R. Soc. London*, *A165*, 476–484.

Tompkins, A. M. (2002), A prognostic parameterization for the subgrid-scale variability of water vapor and clouds in large-scale models and its use to diagnose cloud cover, *J. Atmos. Sci.*, *59*, 1917–1942.

Wood, R., and D. L. Hartmann (2006), Spatial variability of liquid water path in marine low cloud: the importance of mesoscale cellular convection, *J. Clim.*, *19*, 1748–1764.

Xie, S., et al. (2010), Clouds and more: ARM climate modeling best estimate data—A new data product for climate studies, *Bull. Am. Meteorol. Soc.*, *91*, 13–20, doi:10.1175/2009BAMS2891.1.

Zhang J., U. Lohmann, and B. Lin (2002), A new statistically based autoconversion rate parameterization for use in large-scale models, *J. Geophys. Res.*, *107*(D24), 4750, doi:10.1029/2001JD001484.